Available online at www.sciencedirect.com
SCIENCE DIRECT
Journal of Solid State Chemistry 179 (2006) 2237–2244
JOURNAL OF SOLID STATE CHEMISTRY
www.elsevier.com/locate/jssc

Rapid communication

Correlation of reactivity with structural factors in a series of Fe(II) substituted cobalt ferrites

Elsa E. Sileo[a], Luis García Rodenas[b,c], Carlos O. Paiva-Santos[d], Peter W. Stephens[e], Pedro J. Morando[b,c,f,*], Miguel A. Blesa[b,f,g]

[a]*INQUIMAE, Departamento de Química Inorgánica, Analítica y Química Física, Facultad de Ciencias Exactas y Naturales, Universidad de Buenos Aires, Pabellón II, Ciudad Universitaria, C1428EHA, Buenos Aires, Argentina*
[b]*Unidad de Actividad Química, Centro Atómico Constituyentes, Comisión Nacional de Energía Atómica, Avenida General Paz 1499, 1650 San Martín, Provincia de Buenos Aires, Argentina*
[c]*Instituto de Tecnología J. Sábato, Universidad Nacional de San Martín, Avenida Gral. Paz 1499, 1650 San Martín, Provincia de Buenos Aires, Argentina*
[d]*Instituto de Química, Universidade Estadual Paulista,UNESP. Araraquara, 14801-970, São Paulo, Brazil*
[e]*Department of Physics and Astronomy, Stony Brook University, Stony Brook, NY 11794-3800, USA*
[f]*National Research Council of Argentine (CONICET), Avenida Rivadavia 1917, C1033AAJ Buenos Aires, Argentina*
[g]*Escuela de Posgrado, Universidad Nacional de San Martín, Peatonal Belgrano 3563 1er Piso, 1650 San Martín, Provincia de Buenos Aires, Argentina*

Received 2 January 2006; received in revised form 21 March 2006; accepted 26 March 2006
Available online 4 April 2006

Abstract

A series of powdered cobalt ferrites, $Co_xFe_{3-x}O_4$ with $0.66 \leqslant x < 1.00$ containing different amounts of Fe^{II}, were synthesized by a mild procedure, and their Fe and Co site occupancies and structural characteristics were explored using X-ray anomalous scattering and the Rietveld refinement method. The dissolution kinetics, measured in 0.1 M oxalic acid aqueous solution at 70 °C, indicate in all cases the operation of a contracting volume rate law. The specific rates increased with the Fe^{II} content following approximately a second-order polynomial expression. This result suggests that the transfer of Fe^{III} controls the dissolution rate, and that the leaching of a first layer of ions Co^{II} and Fe^{II} leaves exposed a surface enriched in slower dissolving octahedral Fe^{III} ions. Within this model, inner vicinal lattice Fe^{II} accelerates the rate of Fe^{III} transfer via internal electron hopping. A chain mechanism, involving successive electron transfers, fits the data very well.

Keywords: Cobalt ferrites; X-ray anomalous scattering; Rietveld method; Kinetic dissolution; Electron hopping

1. Introduction

Iron oxides, hydroxides and oxohydroxides containing Fe^{II} and/or Fe^{III} together with O and/or OH constitute a very large family of compounds, of widespread occurrence in nature [1]. Magnetite, Fe_3O_4 ($Fe^{II}Fe^{III}_2O_4$), is an iron oxide possessing the inverse spinel structure. Many cations Me^{II} may substitute for Fe^{II} forming ferrites, a series of isostructural mixed Me^{II}, Fe^{II} and Fe^{III} oxides of general formula $Me_xFe_{3-x}O_4$ ($0 < x \leqslant 1$). For $x = 1$, two types of limiting spinels are defined by the distribution of Me^{II} and Fe^{III} in the octahedral (*A*) and tetrahedral (*B*) sites defined by a cubic close packing of oxide ions. The limiting inverse spinel presents all the Me^{II} ions in the *A* sites, $[Me^{II}_{0.5}Fe^{III}_{0.5}]^A_2[Fe^{III}]^BO_4$, whereas direct spinels are of the type $[Fe^{III}]^A_2[Me^{II}]^BO_4$. For any given Me, the degree of inversion of well annealed stoichiometric ferrites is determined by the intrinsic properties of Me^{II} and Fe^{III}. In particular, $Co^{II}_xFe_{3-x}O_4$ ferrites present variable proportions of Fe^{II} and Fe^{III} ions in the octahedral *B*-sites ($[Co^{II}_{x-a}Fe^{II}_{1-x}Fe^{III}_{1+a}][Co^{II}_aFe^{III}_{1-a}]O_4$) [2]. Ferrites have an extensive application in radio, television, microwave and satellite communications, audio-video and digital recording

*Corresponding author. Unidad de Actividad Química, Centro Atómico Constituyentes, Comisión Nacional de Energía Atómica, Avenida General Paz 1499, 1650 San Martín, Provincia de Buenos Aires, Argentina. Fax: +54 11 6772 7886.
E-mail address: morando@cnea.gov.ar (P.J. Morando).

0022-4596/$ - see front matter © 2006 Elsevier Inc. All rights reserved.
doi:10.1016/j.jssc.2006.03.041

and as permanent magnets [3]. Traditionally, ceramic methods are used to prepare ferrites for these applications; however, soft procedures based on the precipitation of precursors at low temperatures and mild thermal treatment are increasingly more frequent [4,5]. The preparation of nanosized ferrites has recently become an exciting area of fundamental and applied researches in material sciences [6–8].

Cobalt ferrites are formed by crystallization at moderate temperature in the external layer of corrosion products that accumulate on the surface of metals in heat transport piping systems [9]. This formation plays an important role in the transport of radioactivity from the core to out-of-core components of nuclear power stations [10]; furthermore, the dissolution mechanisms of cobalt ferrites in oxalic acid media are of importance in decontamination processes [11,12]. The dissolution of ferrites is also of considerable practical importance in fields as diverse as the extraction of metals from ores and the transport of metals in the hydrologic cycles.

Abundant previous work has addressed the changes in reactivity of a given powdered metal oxide caused by changes in the composition of the aqueous solution. It has been amply documented that low valence (reducing) metal ions accelerate the dissolution of Fe^{III} oxides [13,14] and that dissolved Fe^{II} catalyses the dissolution [15,16]. In both cases, heterogeneous electron transfer is involved. Studies on a series of different solids are on the other hand scanty because the synthetic method has to be controlled very precisely to avoid reactivity changes due to differences in particle morphology and other features of the solid. Thus, any attempt to explore trends in a series of ferrites must take into account the possible changes in the degree of inversion. In effect, it has been reported [17] that the inversion can be induced mechanically in zinc ferrite and that the resulting deformation of the octahedral geometry may be correlated with an increase in the dissolution rate in diluted acids.

Some years ago we showed that the dissolution rate of cobalt ferrites $Co_xFe_{3-x}O_4$ in aqueous thioglycolic acid (TGA) was highly sensitive to x, an abrupt decrease in reactivity being observed for $x>0.70$ [18]. This result was interpreted in terms of a possible correlation between the dissolution mechanism and the electrical conductivity through electron hopping in octahedral Fe^{II} and Fe^{III} ions.

This paper explores and discusses this hypothesis, using a series of cobalt ferrites $Co_xFe_{3-x}O_4$ with $0.66\leqslant x<1.00$ that contain different amounts of Fe^{II}. The Fe and Co site distributions were measured by X-ray anomalous scattering and Rietveld [19] refinement simulations. The materials thus prepared were shown to have the same specific surface area, particle morphology and a similar degree of inversion, thus allowing their use to probe the influence of Fe^{II} content on the dissolution kinetics in aqueous media.

A typical aggressive reagent, oxalic acid, was chosen for this purpose. The results demonstrate that the degree of substitution affects the reactivity and it is postulated that electron hopping in octahedral Fe^{II} and Fe^{III} ions is the causative factor for the observed behavior.

2. Experimental

2.1. Sample preparation and analysis of the solids

Spherical cobalt ferrite particles of narrow size distribution were prepared using a modified procedure which was developed earlier by Tamura and Matijević [20]. KOH (0.08 mol) and KNO_3 (0.16 mol) were added to a cylindrical reaction vessel containing 750 cm^3 of double-distilled water. N_2 was bubbled through the solution for 2 h and 50 cm^3 of a solution containing $FeSO_4$ and $Co(NO_3)_2$ were poured into the vessel. The total amount of metal ions was kept constant at 0.04 mol and the molar ratio [Co]:[Fe] was varied in each preparation. The reaction vessel containing the coprecipitated $Fe(OH)_2$ and $Co(OH)_2$ was immersed in a bath at 90 °C and the solids were aged for 4 h with continuous stirring and N_2 purge. The solids were filtered through Millipore membranes (0.45 μm pore size), heated for 1 h at 700 °C and then cooled to room temperature in an air atmosphere.

Fe and Co contents in the prepared samples and in the dissolution experiments were measured spectrophotometrically using TGA [21] in a Shimadzu UV-210A spectrophotometer and by atomic absorption spectrometry in a Perkin Elmer A Analyst 100 apparatus, respectively. Particle morphology and size were characterized by scanning electron microscopy (SEM) using a Phillips SEM 500 apparatus, and near-surface composition was determined by EDS, albeit the results demonstrated that the probed volume lead essentially to bulk concentration ratios. Specific surface area (BET method) measurements were obtained in a Micromerities AccuSorb 2100 E equipment. Preliminary diffraction patterns were recorded in a Siemens D5000 diffractometer.

2.1.1. X-ray anomalous scattering

The mixed oxides $Co_xFe_{3-x}O_4$ were characterized by measurements of high-resolution powder diffraction. Data were collected at the SUNY X3B1 beam line at the National Synchrotron Light Source, Brookhaven National Laboratory. In the anomalous scattering experiments, two sets of measurements were collected at different X-rays wavelengths. The first one was collected at $\lambda_1 = 1.74671(2)$ Å, near the absorption edge of the Fe atom. At this energy the anomalous scattering factor f' for Fe and Co differ markedly, being −6.006 and −2.288 [22], respectively. The second set was collected at $\lambda_2 = 0.69948(2)$ Å; at this remote point from the absorption edge of Fe, both f' factors are similar being 0.346 and 0.349 for Fe and Co, respectively.

Radiation was selected by a double Si(111) monochromator. Both wavelengths and the zero point have been calibrated from seven well-defined reflections of a NIST1976 flat-plate alumina standard. The diffracted

beam was analyzed with a Ge(111) crystal and detected with an Na(Tl)I scintillation counter with a pulse-height discriminator in the counting chain. The incoming beam was monitored by an ion chamber for normalization of the decay of the primary beam. In the parallel-beam configuration, the resolution is determined by the analyzer crystal instead of by slits. Data were collected at room temperature. Measurements at λ_1 were recorded in the 2θ range 33.90–115.98° with scanning steps of 0.02° and a counting time of 2.0 s. Data collection range, scanning step and counting time for measurements at λ_2 were 8.00–51.99°, 0.01°, and 1.5 s, respectively.

2.1.2. X-ray diffraction refinement

Powder data were input directly into the GSAS structure refinement code [23] under the EXPGUI interface [24] implementing the Rietveld technique [19]. For each sample, the two patterns collected at different wavelengths were refined simultaneously. Scattering factors for fully ionized species were used in the refinements.

Starting unit-cell parameters and atomic coordinates for cobalt ferrite [25] and hematite [26] were taken from literature. In the first steps of the refining procedure, only Fe^{3+} was situated in the metal positions of the ferrite structure and in the final steps the occupancy of the sites was refined allowing the substitution of Fe for Co.

The measured background was fitted by a polynomial function. Peak profiles were fitted using the Thompson-Cox-Hastings pseudo-Voigt function [27] with the microstrain broadening description of Stephens [28]. Cell parameters and sample displacement, full width at half maximum, microstrain broadening parameters for the peak shape, scale factor, positional and isotropic thermal parameters were also refined for all atoms.

2.2. Kinetic studies

Kinetic experiments were performed in the dark under N_2 in a magnetically stirred vessel immersed in a thermostat at 70.0 ± 0.1 °C. In a typical experiment, the oxide (ca. 20 mg) was poured over 100 cm^3 of 0.1 M oxalic acid solution. Ionic strength was fixed at 0.5 M with $NaClO_4$ and pH was set at 3.5. At adequate time intervals, samples of 1 cm^3 were taken and filtered through a 0.45-μm cellulose acetate membrane. Total Fe and Co in the filtrate were measured as described at the beginning of this section.

The total Fe and Co concentration data, used to characterize the dissolution kinetics of the ferrite phase, were corrected by subtracting the Fe and Co concentrations reached during a preset previous stage during which the measured Fe/Co concentration ratio largely exceeds the value for the ferrite. In this stage, a hematite surface layer (see below) is completely removed.

3. Results and discussion

3.1. Characterization of the solids

Table 1 summarizes the data obtained by chemical analyses and Rietveld simulation of the anomalous X-ray diffraction data, together with their associated errors. The bulk chemical composition of each sample, determined by triplicate, reflects the existence of a small fraction of hematite whose presence is shown by the diffraction experiment. The ferrite-to-hematite weight ratio is indicated in the third column of Table 1; the almost stoichiometric ferrite sample $Co_{0.998(11)}Fe_{2.002(11)}O_4$ contains the highest amount of hematite, 11.04(13) wt%. EDS in this case indicate a weight ratio Fe/Co = 2.19 corresponding to 10 wt% hematite, in agreement with the large sampling volume of the technique that leads to approximate bulk concentration values. The dissolution behavior, on the other hand, demonstrated that in the early stages, Fe dissolution is much faster than Co dissolution, indicating the existence of a thin hematite layer, as also found in previous work [29] on nickel ferrite particles synthesized by a similar wet procedure. The formation of a hematite layer in the last stages of particle growth may be due to the solubility of Co^{II} that leaves some unbalanced Fe^{III}. Due to the small particle size and the small thickness of the outermost layer, the distribution of both phases does not affect the accuracy of the X-ray data. Ancillary PDRX measurements were carried out with samples treated with oxalic acid to remove the outer layer. The hematite diffraction peaks disappear when 15% of the solid was dissolved. The detailed structural characterization was not

Table 1
Chemical analysis, phases weight ratio and site occupancies in the series

Sample	Co:Fe (mol/mol) bulk	Wt% ferrite/ hematite	Site occupancies (ferrite phase)	Refined formula (ferrite phase) $Co_xFe_{3-x}O_4$	Co:Fe (mol/ mol) (ferrite)	$x_{Fe^{II}} = 1 - x$	Inversion degree (Λ)
1	0.478	88.96(3)/11.04(13)	$(Fe_{0.820(7)},Co_{0.180(7)})$ $(Fe_{0.591(2)}Co_{0.409(2)})_2O_4$	$Co_{0.998(11)}Fe_{2.002(11)}O_4$	0.498 ± 0.008	0.002 ± 0.011	0.82 ± 0.04
2	0.351	97.20(4)/2.80(4)	$(Fe_{0.895(6)},Co_{0.105(6)})$ $(Fe_{0.649(2)}Co_{0.351(2)})_2O_4$	$Co_{0.807(10)}Fe_{2.193(10)}O_4$	0.368 ± 0.006	0.193 ± 0.013	0.89 ± 0.03
3	0.306	92.23(2)/7.77(20)	$(Fe_{0.895(6)},Co_{0.105(6)})$ $(Fe_{0.703(3)}Co_{0.297(3)})_2O_4$	$Co_{0.699(12)}Fe_{2.301(12)}O_4$	0.303 ± 0.007	0.301 ± 0.015	0.89 ± 0.03
4	0.276	95.11(2)/4.89(10)	$(Fe_{0.859(5)},Co_{0.141(5)})$ $(Fe_{0.742(4)}Co_{0.258(4)})_2O_4$	$Co_{0.659(13)}Fe_{2.341(13)}O_4$	0.281 ± 0.007	0.341 ± 0.014	0.86 ± 0.03

repeated with the pickled sample because the results obtained with the original particles were accurate enough for our purposes.

It is frequent that thin layers of another phase form on the surface of particles grown in aqueous media because of the changing solution conditions during growth. It is essential to take this fact into account when using particles obtained by soft procedures. In the best cases (e.g. simple stoichiometric oxides) the surface layer may simply be hydroxylated. In mixed oxides it is often found that the rate of incorporation of the two metals to the solid lattice differ and hence changes in composition with depth ensue. Thus, Perriat et al. [30] showed that the surface of $Fe_{3-x}Ti_xO_4$ prepared using a (different) soft procedure is enriched in Ti. In this case, it was possible to remove the compositional heterogeneity by adequate thermal treatment. Interestingly, the oxidation of this material leads to the formation of a hematite surface layer [31], whereas the oxidation of $Cd_xFe_{3-x}O_4$ produces a maghemite layer [32].

The structural characterization of the original material was not only possible; it also permitted to adequately design the experiments carried out to study the kinetic behavior of the majority bulk ferrite phase, on which this paper focuses.

The refined cation distribution is shown in the fourth column; from these values, the bulk ferrite formula (fifth column) and the Co/Fe ratio (sixth column) are obtained. The cation distribution refinement of the series shows that Co occupies both sites in variable proportions. Tetrahedral and octahedral Co occupancies varies from 0.105(6) to 0.180(7) and 0.258(4) to 0.409(2), respectively. The contents of Fe^{II} in the octahedral sites, calculated from the Co substitution degree ($x_{FeII} = 1 - x$) and their propagated error limits are given in the seventh column. The amount of Co^{III} cations in cobalt ferrites is negligible as the reaction $Fe^{II} + Co^{III} \rightarrow Fe^{III} + Co^{II}$ is strongly shifted to the right [33].

The inversion degree Λ, defined as the fraction of tetrahedral sites occupied by Fe^{III} atoms, is also given in Table 1. The Λ range, from 0.82 to 0.89, agrees with the partially inverse nature of cobalt ferrites [34,35].

Table 2 shows the quality of the fitting; the total reliability factors R_{wp}, R_p and G_{ofF} values between 8.33–8.94, 5.47–6.26 and 1.39–1.49 are reasonably adequate. The ferrite cell parameter, in the range of 8.3722(1)–8.3849(1) Å, increases with total cobalt content. The last lattice parameter value is close to that of $CoFe_2O_4$ [25]. Also, the hematite cell parameters are close to pure-hematite reported values ($a = b = 5.034$ and $c = 13.750$ Å) [36].

Our approach for the following analysis does not take into account the possible presence of cation vacancies in the ferrite. The synthesis procedure guarantees that the concentration of vacancies in the whole series is constant. Deviations from the condition $\delta = 0$ would imply small shifts in the calculated inversion degrees (see Table 1) without changing the observed trends.

Fig. 1(a) and (b) compare the experimental and the calculated diffraction patterns at both wavelengths for sample 1 ($x = 0.998$) and shows that the structural model fits the data well. The changes in the intensity ratios for two different peaks observed in Fig. 1(a) and (b) follow the expected trends when the anomalous scattering technique is applied.

The specific surface area measured by gas adsorption (BET) is $3.88 \pm 0.03\ m^2\ g^{-1}$ for all the prepared solids. The SEM pictures of all samples show spherical and monodisperse particles with diameters in the order of 0.3 μm. Fig. 2 corresponding to the sample with $x = 0.998$ is shown as an example. In the SEM picture, hematite and ferrite phases cannot be differentiated; however, XRD measurements taken before and after partial oxalic acid dissolution show that a hematite layer is covering the ferrite particles.

Fig. 3 shows the changes in cell parameter with increasing Fe^{II} content. The unit cell parameter decreases with the increment in the Fe^{II} content and a deviation from the linearity predicted by Vegard's law is observed. This fact could be accounted by the presence of Co^{II} ions in

Table 2
Agreement factors for the refinements and lattice parameters

Sample	R_{wp}	R_p	G_{ofF}	R_B (Histg. λ_1/ Histg. λ_2)	$a = b = c$ (Å) (ferrite)	$a = b$ and c (Å) (hematite)
1	8.64	5.95	1.41	3.07/1.88	8.3849(1)	5.0347(1) 13.7464(1)
2	8.33	5.47	1.49	2.89/1.71	8.3755(1)	5.0351(1) 13.7452(5)
3	8.94	6.26	1.39	4.95/1.82	8.3726(1)	5.0345(1) 13.7461(3)
4	8.70	6.02	1.43	5.12/2.26	8.3722(1)	5.0348(1) 13.7470(3)

$R_p : 100 \sum |I_o - I_c| / \sum I_o$, $R_{wp} : 100 \left[\sum w_i (I_o - I_c)^2 / \sum w_i I_o^2\right]^{0.5}$, $R_B : 100 \sum |I_{ko} - I_{kc}| / \sum I_{ko}$, $G_{ofF} = \sum w_i (I_o - I_c)^2 / (N - P)$.
I_o and I_c: observed and calculated intensities.
w_i: weight assigned to each step intensity.
I_{ko} and I_{kc}: observed and calculated intensities for Bragg k-reflection.
N and P: number of data points in the pattern and number of parameters refined.

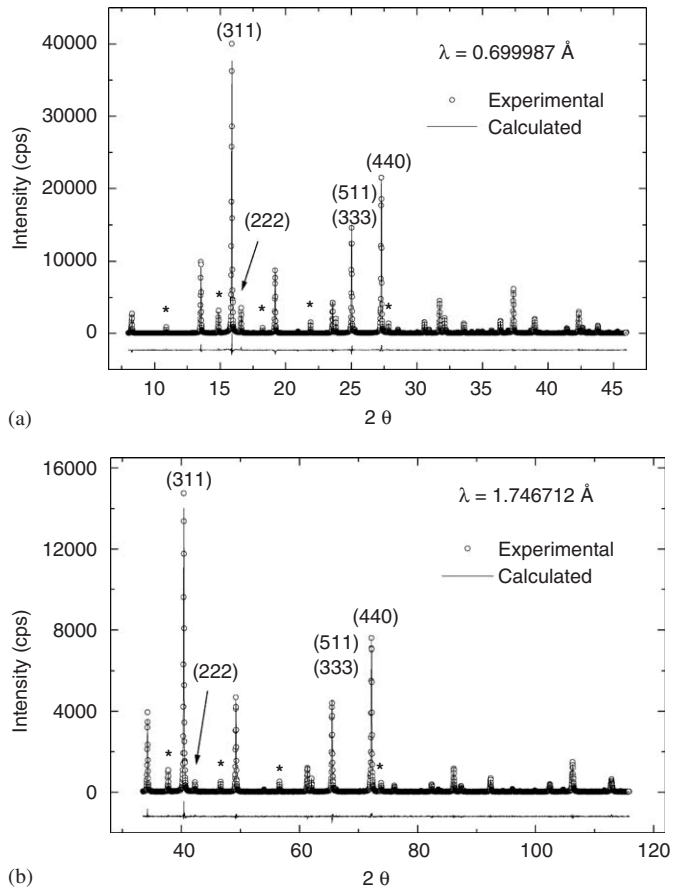

Fig. 1. Experimental and calculated diffraction pattern for sample 1 ($x = 0.998$). The marks (*) identify hematite peaks.

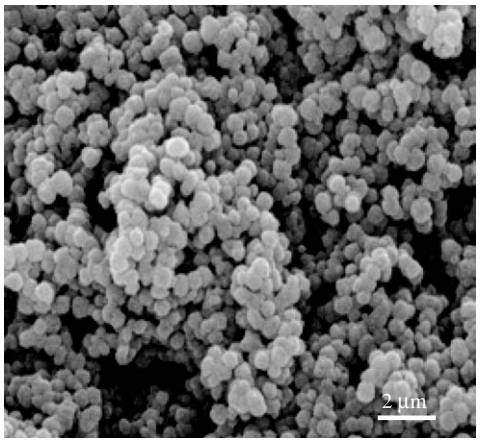

Fig. 2. SEM picture of sample 1 ($x = 0.998$) (magnification 15.400 ×).

both tetrahedral and octahedral sites. In effect, non-linear behaviors have been reported for systems that are not completely normal or inverse [37,38].

3.2. Kinetics of ferrite dissolution in oxalic acid

All samples follow the same dissolution behavior. Up to 40 wt% dissolution, the contracting volume model described by Eqs. (1) and (2) fits the data well. In these

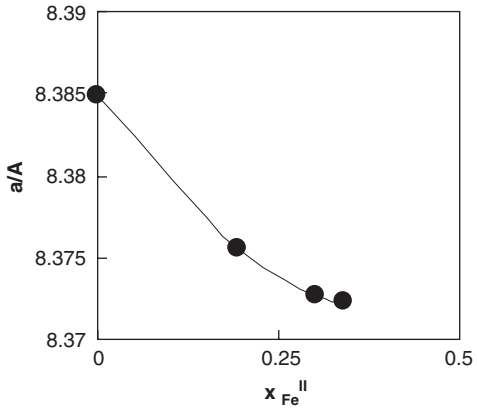

Fig. 3. Changes in the lattice parameter a with increasing Fe^{II} content (●).

equations, S is the instantaneous specific area of the sample, S^o its initial value and k' is the specific rate per unit area (s^{-1}); f stands for the dissolved fractions of both iron and cobalt, $f_{Me} = w/w_o$ (where Me = Fe or Co, w is the mass of dissolved Me at time t and w_o is the initial mass). Fig. 4 shows the plots corresponding to Eq. (2) for Me = Fe. The data of each kinetic runs fit Eq. (2) with $R \geqslant 0.98$ and the reproducibility between duplicates was within 2.5%. The build up of Co is equivalent at all times (congruent dissolution) as shown in the inset to Fig. 4. For comparison, the figure also shows the negligible dissolution observed in a solution of $HClO_4$ at pH 3.5.

$$df_{Me}/dt = k'S(t) = k'S^o(1 - f_{Me})^{2/3}, \quad (1)$$

$$1 - (1 - f_{Me})^{1/3} = (k'/3)t. \quad (2)$$

The specific rate of iron dissolution, k (mol Fe m^{-2} s^{-1}), is proportional to k' as shown in Eq. (3), where M_{Fe} is the relative atomic weight of iron and $(3-x)$ is the total content of Fe in the ferrite phase:

$$k = k'/S^o(3 - x)M_{Fe}. \quad (3)$$

Changes in k with the composition of the solid are shown in Table 3. The dissolution rate decreases with the increase in cobalt content and the variations on the dissolution specific rates may be correlated with the Fe^{II} content.

Tkáčová et al. [17] correlated the reactivity of zinc ferrites with the inversion degree; however, in our case, the inversion degree is approximately constant (see Table 1) and the reactivity trends in the series should be explained by the Fe^{II} fraction in the octahedral sites.

Several previous works have amply documented that the dissolution rate of Fe^{III} oxides in oxalic acid is enhanced by the presence of Fe^{II} in the liquid phase. The increase in dissolution rate is mediated by a heterogeneous charge transfer step [15,16] between ferrous-oxalate complexes and surface ferric ions according to

$$\equiv Fe^{III} - C_2O_4^{2-}(H^+) + \{Fe^{II} - C_2O_4^{2-}(H^+)\}_{aq} \rightarrow$$
$$\equiv Fe^{II} - C_2O_4^{2-}(H^+) + \{Fe^{III} - C_2O_4^{2-}(H^+)\}_{aq}. \quad (4)$$

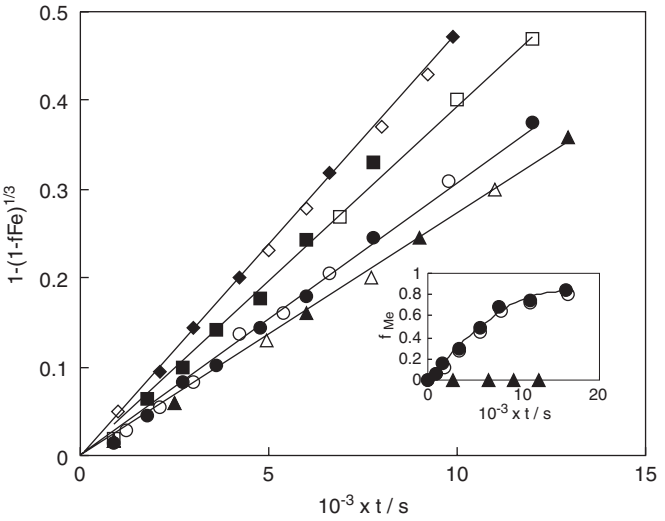

Fig. 4. Contracting volume linear kinetic plots for the dissolution of $Co_xFe_{3-x}O_4$ with $x = 0.998$ (▲), (△); 0.807 (●), (○); 0.699 (■), (□); 0.659 (◆), (◇). Duplicate runs are represented by full and empty symbols. Inset: time dependence of cobalt (○) and iron (●) dissolution factors for sample 1 ($x = 0.998$); results in $HClO_4$ solution (▲) are shown for comparison.

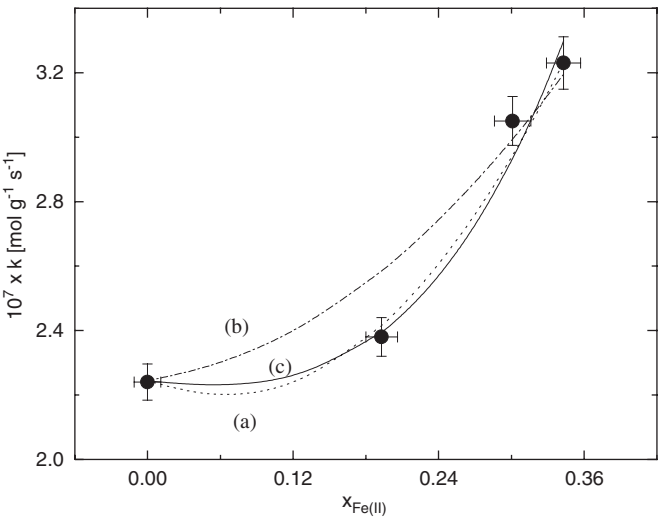

Fig. 5. Specific dissolution rates as a function of the Fe^{II} content of the solid. Curve a was calculated from the empirical Eq. (5); curve b from Eq. (8), assuming five next neighbors from the solid attached to the dissolving unit ($n = 5$); and curve c from Eq. (9), with $n = 5$ and accepting a propagating chain of five terms, as described in the text.

Table 3
Specific rates according to the contracting volume model in 0.1 M oxalic acid at 70.0 °C, pH = 3.5 for ferrites of various Fe^{II}/Fe^{III} relationships

Ferrite (refined formula)	(Fe^{II}/Fe^{III}) octahedral	$10^7 \times k$ (mol Fe m^{-2} s^{-1})
$Co_{0.998}Fe_{2.002}O_4$	0.001 ± 0.009	2.24 ± 0.06
$Co_{0.807}Fe_{2.193}O_4$	0.174 ± 0.010	2.39 ± 0.06
$Co_{0.699}Fe_{2.301}O_4$	0.272 ± 0.012	3.05 ± 0.07
$Co_{0.659}Fe_{2.343}O_4$	0.300 ± 0.013	3.24 ± 0.08

The greater lability of Fe^{II}–O bonds compared to that of Fe^{III}–O bonds makes the subsequent phase transfer faster. In the case of Fe^{II} containing Fe^{III} oxides, dissolution is accompanied by the leaching of Fe^{II} into the solution [16,39]. Once the build up of Fe^{II} reaches a critical amount, a fast reductive dissolution takes place, giving rise to acceleratory dissolution profiles.

In our case, dissolution is not acceleratory, thus ruling out the participation of dissolved Fe^{II}. The minor structural changes (lattice parameters) cannot be responsible for the observed trend; the largest changes in rate are found in the substitutional range in which the smallest changes in the cell parameter a are found.

Electronic effects within the solid framework provide a good rationale for the results presented in Fig. 5. As the electron hopping between adjacent Fe^{II}–Fe^{III} pairs in octahedral holes and the transfer of ions from the tetrahedral sites to solution are both fast processes, we propose that:

1. The transfer of ions from octahedral sites controls the dissolution rate.
2. As the transfer of Fe^{II} to the solution is faster than that of Fe^{III} [15,16], the leaching of a first layer of divalent ions (Co^{II}, Fe^{II}) leaves exposed a surface enriched in slower octahedral Fe^{III} ions; the transfer of these is the rate determining step.
3. Dissolution via Fe^{III} ions that do not have adjacent Fe^{II} in octahedral sites proceeds at the rate measured for stoichiometric ferrite.
4. Octahedral Fe^{II} ions accelerate the transfer of adjacent superficial Fe^{III} through an internal electron transfer $\{\equiv Fe^{II}_{(1)} \equiv Fe^{III}_{(2)}\} \leftrightarrow \{\equiv Fe^{III}_{(1)} \equiv Fe^{II}_{(2)}\}$, mechanism that labilizes Fe^{III}. Thus, Fe^{III} ions are transferred to the solution at a higher rate.
5. A propagating chain may be established when Fe^{II}–Fe^{III} pairs are available in the inner layers of the solid.

Eq. (5) indicates the empirical quadratic correlation found between the specific rates and $x_{Fe^{II}}$, as shown in the curve a of Fig. 5. The figure also includes the two fitting curves discussed below.

$$k = 2.24 \times 10^{-7} - 1.70 \times 10^{-7} x_{Fe^{II}} + 1.34 \times 10^{-6} \left(x_{Fe^{II}}\right)^2. \quad (5)$$

We shall first consider that acceleration is due to the effect described in point 4 only (step 5 is not yet considered). The probability P of finding at least one octahedral cluster Fe^{III}–Fe^{II} in the surface can be calculated as

$$P = \left\{1 - \left[1 - \left(a_{Fe^{II}}/6\right)\right]^n\right\}. \quad (6)$$

In Eq. (6), $a_{Fe^{II}}$ is the average number of Fe^{II} in the octahedral holes adjacent to a given Fe^{III} ion in bulk; n, the number of adjacent octahedral sites surrounding a dissolving surface Fe^{III} ion. This number is expected to be

between 3 and 5 [10]; for a kink, $n = 3$, whereas for a flat 100 surface, $n = 5$. The bracket in Eq. (6) accounts for the probability of not finding an adjacent Fe^{II}. For spinels with high inversion degree, Fe^{III} occupies half of the six vicinal octahedral positions in the bulk and Co^{II} and Fe^{II} take the remaining three positions in proportions defined by their mole fractions. At low Fe^{II} contents, the polynomial expression for Eq. (6) can be truncated in the first term, thus yielding Eq. (7). Truncation in the quadratic term is physically meaningless (the sign of the term in $(x_{Fe^{II}})^2$ is negative) and must contain an odd number of terms.

$$P = n(a_{Fe^{II}}/6) = (n/2)x_{Fe^{II}}. \quad (7)$$

For the mechanism described by steps 1–4 above, the specific rate can be written as the sum of two terms, one accounting for normal dissolution (step 3) and the other one accounting for the enhancement just described. In Eq. (8), k_{Co} and k_{Fe} stand for the specific rate constants for non-enhanced and enhanced Fe^{III} phase transfer, respectively:

$$k = k_{Co}x_{Co^{II}} + k_{Fe}x_{Fe^{II}}\left[1 + (n/2)(x_{Fe^{II}})\right] = k_{Co} + (k_{Fe} - k_{Co})x_{Fe^{II}} + (n/2)k_{Fe}(x_{Fe^{II}})^2. \quad (8)$$

Curve b in Fig. 5 shows the best fitting of Eq. (8), with $k_{Co} = 2.24 \times 10^{-7}$ mol m^{-2} s^{-1}, $k_{Fe} = 2.70 \times 10^{-7}$ mol m^{-2} s^{-1} and $n = 5$. It is seen that the fitting is worse than that of the empirical Eq. (5). Note that although both equations have three adjustable parameters, n can be varied only within narrow limits and does not influence much the fitting. In practice, Eq. (8) is close to being a two parameter expression.

The derivation of (8) assumes that electron hopping to Fe^{III} takes place from adjacent Fe^{II} and that upon dissolution, Fe^{II} ions cannot transfer the electron back to the solid. This assumption is valid as long as the concentration of dissolved Fe^{II} is low enough to make the heterogeneous electron transfer pathway negligible.

However, the model is too restrictive because as long as electron hopping can take place and is not interrupted by Co^{II} centers, the electron chain may involve more atoms. This possibility, described by tenet 5 above and not taken into account in Eq. (8), leads to Eq. (9):

$$k = k_{Co} + (k_{Fe} - k_{Co})x_{Fe^{II}} + (n/2)k_{Fe}(x_{Fe^{II}})^2 \times \left[1 + (n/2)x_{Fe^{II}} + \left[(n/2)(x_{Fe^{II}})\right]^2 + \ldots\right]. \quad (9)$$

Curve c in Fig. 5 demonstrates that an excellent fitting of the data can be achieved by accepting three terms in the summation within brackets, with $k_{Co} = 2.24 \times 10^{-7}$ mol m^{-2} s^{-1}, $k_{Fe} = 1.65 \times 10^{-7}$ mol m^{-2} s^{-1}, $n = 5$ and truncation of the square bracket in the quadratic term. Although the actual value of the chain length is subjected to a large error, experimental data do indeed suggest a propagating chain. The rate of dissolution of magnetite (the end member of the series, with $x_{Fe^{II}} = 1$) is unknown; the fast buildup of dissolved Fe^{II} triggers the pathway mediated by heterogeneous electron transfer. However, the shape of the f/t plots [16,39] requires intrinsic specific rates of dissolution larger than those found for the present ferrites and a long propagating chain. Magnetite dissolution profiles are so abrupt that they seem to indicate massive dissolution mediated by the phase transfer of a small fraction of Fe^{II} atoms. A good model would therefore probably follow the ideas of chains propagating in the solid with a given probability of branching and of death, as proposed by Delmon [40] in a different context.

The modeling of the data yields $k_{Fe} < k_{Co}$. This result indicates that the acceleration effect of Fe^{II} is due only to electron hopping, and not to simple ionic polarization effects.

Appreciable conductivity in ferrites requires fast electron hopping between Fe^{III} and Fe^{II} in octahedral sites; thus, magnetite is metallic or a degenerate semiconductor [41–43], whereas $ZnFe_2O_4$ is an insulator. Resistivity data of $Zn_xFe_{3-x}O_4$ ($0 < x \leqslant 0.9$) are complementary to the results shown in Fig. 5, as they show the abrupt decrease in conductivity when the substitution degree in magnetite reaches $x \cong 0.7$ [42]; for $x < 0.6$, a saturation value, similar to that of magnetite is reached. Mössbauer data shows a similar behavior of $Ni_xFe_{3-x}O_4$, although in this case further decrease of the degree of substitution produces further increases in the conductivity [43]. In the case of $Co_xFe_{3-x}O_4$ the Mössbauer hyperfine fields show that electron hopping between adjacent octahedral Fe^{III}–Fe^{II} is fast [44,45]. In the range $x < 0.7$ this exchange is unrestricted [43], whereas for higher values of x the amount of adjacent pairs decreases rapidly [44]. These results are in agreement with our earlier work [18], which showed that the dissolution rate of $Co_xFe_{3-x}O_4$ in TGA decreases sharply when the Co contents reaches 0.7.

4. Conclusion

The incidence of structural factors on the reactivity of solids is not easy to probe, because changes in particle area, morphology, etc., compound on possible structural effects. Thus, it has been more frequent to deal with the reactivity of one given solid sample (identical composition and history) towards a series of dissolution reagents. The present case gives a nice example of the importance that electron hopping between adjacent octahedral Fe^{III}–Fe^{II} pairs bears in the reductive dissolution behavior of $Co_xFe_{3-x}O_4$ for various x values.

Acknowledgments

Work supported by Agencia Nacional de Promoción de Ciencia y Tecnología of Argentina (Project PICT 06-06631), Comisión Nacional de Energía Atómica (CNEA), Projects P5-036-01 and P5-036-4. Work performed in part at the National Synchrotron Light Source, Brookhaven National Laboratory, which is supported by the US Department of Energy, Division of Materials Sciences

and Division of Chemical Sciences, under Contract No. DE-AC02-98CH10886.

References

[1] U. Schwertmann, R.M. Cornell, Iron oxides in the laboratory. Preparation and characterization, VCH Publishers, Weinheim, New-York, 1991.
[2] M.K. Fayek, A.A. Bahgat, Z. Phys. B-Condens. Matter 46 (1982) 199.
[3] B. Viswanathan, V.R.K. Murthy, Ferrite Materials, Springer, Berlin, 1990.
[4] B.S.J. Randhawa, J. Mater. Chem. 10 (2000) 2847.
[5] B. Antic, A. Kremenović, A.S. Nikolic, M. Stoiljkovic, J. Phys. Chem. B 108 (34) (2004) 12646.
[6] J.F. Hochepied, P. Bonville, M.P. Pileni, J. Phys. Chem. B 104 (5) (2000) 905.
[7] T. Hyeon, Y. Chung, J. Park, S. Seong Lee, Y.-W. Kim, B.H. Parks, J. Phys. Chem. B 106 (27) (2002) 6831.
[8] K.V.P.M. Shafi, Y. Koltypin, A. Gedanken, R. Prozorov, J. Balogh, J. Lendvai, I. Felner, J. Phys. Chem. B 101 (33) (1997) 6409.
[9] A.K. Vijh, J.W. Diggle, Oxides and Oxides Films, vol. 2, Marcel Dekker, New York, 1973.
[10] M.A. Blesa, A.J.G. Maroto, A.E. Regazzoni, in: Proceedings of the Japan Atomic Industrial Forum, Fukuki City, Japan, 1991.
[11] J.A. Ayres, Decontamination of Reactors and Equipment, Ronald Press, New York, 1970.
[12] M.M. Osterhout, Decontamination and Decommissioning of Nuclear Facilities, Plenum Press, New York, 1980.
[13] M.G. Segal, R.M. Sellers, J. Chem. Soc. Chem. Commun. 21 (1980) 991.
[14] M.G. Segal, R.M. Sellers, J. Chem. Soc. Faraday Trans. I 78 (1982) 1149.
[15] M.A. Blesa, P.J. Morando, A.E. Regazzoni, Chemical Dissolution of Metal Oxides, CRC Press, Boca Raton, FL, 1994.
[16] M.A. Blesa, H.A. Marinovich, E.C. Baumgartner, A.J.G. Maroto, Inorg. Chem. 26 (1987) 3713.
[17] K. Tkáčová, V. Šepelák, N. Števulová, J. Solid State Chem. 123 (1996) 100.
[18] M.A. Blesa, A.J.G. Maroto, P.J. Morando, J. Chem. Soc. Faraday Trans. I 82 (1986) 2345.
[19] H.M. Rietveld, J. Appl. Crystallogr. 2 (1969) 65.
[20] H. Tamura, E. Matijević, J. Coll. Int. Sci. 90 (1981) 100.
[21] D.L. Leussing, N. Newman, J. Am. Chem. Soc. 78 (1956) 552.
[22] D. Waasmaier, A. Kirfel, Acta Crystallog. A 51 (1995) 416.
[23] A.C. Larson, R.B. Von Dreele, General Structure Analysis System (GSAS), Los Alamos National Laboratory Report LAUR 86-748, 1994.
[24] B.H. Toby, J. Appl. Cryst. 34 (2001) 210.
[25] I. Malats, A. Riera, G. Pourroy, P. Poix, J. Alloys Comp. 292 (1993) 113.
[26] E.N. Maslen, V.A. Streltsov, N.R. Streltosova, N. Ishizawa, Acta Crystallog. B 50 (1994) 435.
[27] P. Thompson, D.E. Cox, J.B. Hastings, J. Appl. Crystallogr. 20 (1987) 79.
[28] P.W. Stephens, J. Appl. Crystallogr. 32 (1999) 281.
[29] C.A. Figueroa, E.E. Sileo, P.J. Morando, M.A. Blesa, J. Colloid Interf. Sci. 225 (2000) 403.
[30] P. Perriat, E. Fries, N. Millot, B. Domenichini, Solid States Ionics 117 (1999) 175.
[31] K. Basset, B. Domenichini, J. Merle, P. Perriat, S. Bourgeois, Eur. Phys. J. Appl. 4 (1998) 157.
[32] B. Gillot, D. Thiebaut, M. Laarj, Thermochim. Acta 342 (1999) 167.
[33] I.-H. Jung, S.A. Decterov, A.D. Pelton, H.M. Kim, Y.B. Kang, Acta Mater. 52 (2004) 507.
[34] M.D. Archer, C.G. Morris, G.K. Yin, J. Electroanal. Chem. 118 (1981) 89.
[35] G.A. Sawatzky, F. van der Wonde, A.H. Morrish, J. Appl. Phys. 39 (1968) 1204.
[36] R.L. Blake, R.E. Hessevick, T. Zoltai, L.W. Finger, Am. Mineral. 51 (1966) 123.
[37] D.C. Kahn, M. Misra, A.R. Das, J. Appl. Phys. 53 (1982) 2722.
[38] A.A. Pandit, S.S. More, R.G. Dorik, K.M. Jadhav, Bull. Mater. Sci. 26 (2003) 517.
[39] E. Borghi, P.J. Morando, M.A. Blesa, Langmuir 7 (1991) 1652.
[40] B. Delmon, Introduction a la Cinétiqué Hétérogène, Technip, Paris, 1969 (Chapter XII).
[41] E.J.W. Verwey, P.H. Haayman, F.C. Romeijn, J. Chem. Phys. 15 (1947) 181.
[42] D.C. Dobson, J.W. Linnet, M.M. Rahman, J. Phys. Chem. Solids 31 (1970) 2727.
[43] J.W. Linnet, M. Rahman, J. Phys. Chem. Solids 33 (1972) 1465.
[44] H. Franke, M. Rosenberg, J. Magn. Magn. Mater. 4 (1977) 186.
[45] H. Franke, M. Rosenberg, Physica B 86–88 (1977) 965.